Electric dipole response of ^{6}He: Halo-neutron and core excitations

D. Mikami,[1,*] W. Horiuchi,[1] and Y. Suzuki[2,3]
[1]*Department of Physics, Hokkaido University, Sapporo 060-0810, Japan*
[2]*Department of Physics, Niigata University, Niigata 950-2181, Japan*
[3]*RIKEN Nishina Center, Wako 351-0198, Japan*
(Received 4 April 2014; revised manuscript received 22 May 2014; published 6 June 2014)

Electric dipole ($E1$) response of ^{6}He is studied with a fully microscopic six-body calculation. The wave functions for the ground and excited states are expressed as a superposition of explicitly correlated Gaussians. Final state interactions of three-body decay channels are explicitly taken into account. The ground state properties and the low-energy $E1$ strength are obtained consistently with observations. Two main peaks as well as several small peaks are found in the $E1$ strength function. The peak at the high-energy region indicates a typical macroscopic picture of the giant dipole resonance, the out-of-phase proton-neutron motion. The transition densities of the lower-lying peaks exhibit in-phase proton-neutron motion in the internal region, out-of-phase motion near the surface region, and spatially extended neutron oscillation, indicating a soft-dipole mode and its vibrationally excited mode. The compressional dipole strength is also examined in relation to the soft-dipole mode.

DOI: 10.1103/PhysRevC.89.064303 PACS number(s): 21.10.Gv, 23.20.−g, 27.20.+n, 24.30.Cz

I. INTRODUCTION

Exploring new phenomena in unstable nuclei has become possible due to intense radioactive beams produced by new facilities. A neutron halo is one of the most attractive phenomena found in some unstable nuclei near the neutron dripline, and has attracted much attention since the discovery of the large matter radius of ^{11}Li [1]. Typical two-neutron halo nuclei are, e.g., ^{6}He [2], ^{11}Li, ^{14}Be [3], and the recently observed ^{22}C [4]. A common feature of these nuclei is a small two-neutron separation energy (S_{2n}) that leads to a large matter radius.

It is known that such weakly bound systems exhibit large $E1$ strength at the low-energy region as often studied through Coulomb breakup reactions [5–7]. As a unique phenomenon in the neutron rich nuclei, the possibility of the soft-dipole mode (SDM) has for a long time been discussed as a vibration of the halo neutrons against the core [8–10], which is a variant of the macroscopic picture of the giant dipole resonance (GDR) such as Goldhaber-Teller [11] and Steinwedel-Jensen [12] models.

These days low-lying $E1$ strength in medium- and heavy-mass nuclei has been studied extensively in its relationship to neutron-skin thickness and neutron matter in a neutron star [13,14]. The low-lying strength is observed in neutron-proton unbalanced nuclei and it is often called a pygmy dipole resonance (PDR) because its strength is much smaller than that of the GDR. However, its excitation mechanism is still controversial concerning whether the mode is SDM, collective, or single-particle excitation.

In this paper, we study the $E1$ response of ^{6}He up to the GDR region, focusing on the possibility of the SDM as well as other $E1$ excitation modes. The low-lying $E1$ strength of ^{6}He was observed by the Coulomb breakup experiment of ^{6}He [5], which found a broad peak in the low-energy region just a few MeV above the $\alpha + n + n$ threshold. An indication of the low-lying peak is also reported in a ^{6}Li(^{7}Li,^{7}Be)^{6}He charge-exchange reaction [15]. Theoretically the $E1$ response of ^{6}He is often studied with a macroscopic $\alpha + n + n$ three-body model [16–21]. However, some theoretical uncertainty exists when the α particle is treated as a point particle. Even if the $\alpha + n + n$ three-body problem is solved accurately, two phase-shift equivalent $\alpha - n$ potentials give different $E1$ strength as shown in Refs. [18,19,21]. To avoid such uncertainties, we study the ^{6}He nucleus in a fully microscopic six-nucleon calculation. The six-body model has another important advantage that the distortion of the α core is naturally taken into account. The distortion or core polarization effect is known to play an important role in binding the halo neutrons of ^{6}He [22]. Bacca *et al.* presented six-body calculations for ^{6}He with the effective interaction hyperspherical harmonics (EIHH) combined with a Lorentz integral transform [23,24]. They obtain two peaks for ^{6}He and speculate the existence of the SDM at the low-lying peak as well as the GDR at the higher peak.

The paper is organized as follows. In Sec. II, our six-body model is formulated. The Hamiltonian, basis functions, and model space adopted in the present work are explained here. We perform a variational calculation to obtain the ground state wave function. Those configurations that are accessible by the $E1$ operator are carefully prepared to take account of all the $E1$ strength of ^{6}He. Results and discussions are presented in Sec. III. First, we show the ground state properties of ^{6}He and discuss its structure in Sec. III A. Next we present the $E1$ strength and analyze important configurations for describing the $E1$ excitation in Sec. III B. A comparison with experimental data is made in Sec. III C. The low-lying $E1$ excitation mode as well as the one in the GDR region are discussed in detail in Sec. III D. Section III E discusses the extent to which the $\alpha + n + n$ three-body picture is validated for ^{6}He. The result on compressional $E1$ strength is shown in Sec. III F. Conclusions are drawn in Sec. IV.

II. METHOD

A. Hamiltonian

The Hamiltonian of an N-particle system is specified by a kinetic energy and an effective two-body interaction between

[*]Present address: Hitachi Solutions East Japan, Ltd., Sendai 980-0014, Japan.

nucleons:

$$H = \sum_{i=1}^{N} T_i - T_{\rm cm} + \sum_{i<j} v_{ij}. \quad (1)$$

The proton-neutron mass difference is ignored in the kinetic energy. The center-of-mass (c.m.) motion of the total system, $T_{\rm cm}$, is excluded, and no spurious c.m. motion appears in the calculation. As the two-body interaction, we employ the central Minnesota (MN) potential [25] that fairly well reproduces the binding energies of $N = 2$–6 systems [26]. No three-body force is included. A spin-orbit interaction is often employed, in addition to the central MN force, to reproduce the splitting of $p_{3/2}$ and $p_{1/2}$ phase shifts of the ^{4}He+n system [27]. That interaction was applied to describe the neutron-halo structure of ^{6,8}He in a microscopic three-body and five-body model [28]. We use, however, only the central MN force because the effective spin-orbit force gives ill behavior as shown in a four-body calculation for ^{4}He [29]. Instead we adjust the strength of odd partial waves by changing one free parameter, u, of the MN potential. The u parameter does not affect the binding energies of $N < 5$ systems that are mainly composed of S state. A choice of u will be discussed later. The Coulomb potential is included. The nucleon mass m_N and the charge constant e used in what follows are $\hbar^2/m_N = 41.47$ MeV fm^2 and $e^2 = 1.440$ MeV fm.

B. Basis functions for bound states

In this work, we solve a many-body Schrödinger equation using a variational method. A bound-state solution of the N-nucleon system with spin parity J^π is expressed in terms of a linear combination of the LS coupled basis functions,

$$\Phi^{(N)\pi}_{(LS)JM_JM_T} = \mathcal{A}\left\{\left[\phi^{(N)\pi}_L \chi^{(N)}_S\right]_{JM_J} \eta_{M_T}\right\}, \quad (2)$$

where $\mathcal{A}$ is the antisymmetrizer, and the square brackets denote the tensor product of angular momentum coupling. The spin function χ_S is given in a successive coupling as

$$\chi^{(N)}_{S_{12},S_{123},\ldots,SM_S} = \left[\ldots\left[\left[\chi_{\frac{1}{2}}(1)\chi_{\frac{1}{2}}(2)\right]_{S_{12}}\chi_{\frac{1}{2}}(3)\right]_{S_{123}}\ldots\right]_{SM_S}. \quad (3)$$

Note that the above spin function forms a complete set provided all possible intermediate spins ($S_{12}, S_{123}, \ldots$) are included for a given S. The isospin function η_{M_T} is expressed with a product of single-particle isospin functions. The function η_{M_T} can also be expressed by a linear combination of Eq. (3), e.g., with total isospin $T = 0, 1, 2$ for ^{4}He and $T = 1, 2, 3$ for ^{6}He.

A choice of the variational trial functions is essential to determine the accuracy of the calculation. We employ the correlated Gaussian (CG) basis [30,31], which is flexible to treat few-body dynamics, e.g., to describe a tail in the asymptotic region as well as clustering [32,33]. Also see a recent review [34] for various powerful applications of the CG. Denoting the nucleon coordinate by $\boldsymbol{r}_i$, we use a set of the Jacobi coordinates, $\boldsymbol{x}_i = \boldsymbol{r}_{i+1} - \sum_{j=1}^{i} \boldsymbol{r}_j/i$ ($i = 1, \ldots, N-1$) but other sets of relative coordinates may be used as well. We introduce a shorthand notation $\boldsymbol{x}$ that is an $(N-1)$-dimensional column vector or an $(N-1)\times 1$ matrix whose ith element is the three-dimensional vector $\boldsymbol{x}_i$. The spatial part $\phi^{(N)\pi}_L$ of Eq. (2) generally takes the form [26,35]

$$F_{LM_L}(v, A, \boldsymbol{x}) = \exp\left(-\tfrac{1}{2}\tilde{\boldsymbol{x}}A\boldsymbol{x}\right)\mathcal{Y}_{LM_L}(\tilde{v}\boldsymbol{x}) \quad (4)$$

with a solid harmonic

$$\mathcal{Y}_{\ell m}(\boldsymbol{r}) = r^\ell Y_{\ell m}(\hat{\boldsymbol{r}}), \quad (5)$$

where A is an $(N-1)\times(N-1)$ positive-definite, symmetric matrix and $\tilde{\boldsymbol{x}}A\boldsymbol{x}$ stands for $\sum_{i,j=1}^{N-1} A_{ij}\boldsymbol{x}_i\cdot\boldsymbol{x}_j$. The tilde indicates the transpose of a matrix. The parameter v is an $(N-1)$-dimensional column vector that defines a global vector (GV), $\tilde{v}\boldsymbol{x}(=\sum_{i=1}^{N-1} v_i\boldsymbol{x}_i)$, which is responsible for describing the angular motion of the system. For ^{6}He with the central MN potential, we only need to consider the lowest L because no channel coupling occurs between states with different L: $L = 0$ for the ground states and $L = 1$ for the $E1$ excited states.

The CG-GV basis (4) explicitly describes correlated motion among the particles through the off-diagonal elements of A and the rotational motion of the system is conveniently described by the GV. Both bound and excited states are expressed by the same functional form. For the bound states, the variational parameters are determined by the stochastic variational method (SVM) [26,35,36]. The wave functions for the excited states are constructed on the basis of single-particle (sp) or cluster excitations as explained in Sec. II C. Most noticeable among several advantages of the CG-GV basis functions is that the functional form of Eq. (4) remains unchanged under an arbitrary linear transformation of the coordinate $\boldsymbol{x}$. Another advantage is that the matrix elements for most operators can be evaluated analytically, which allows us to obtain the matrix elements accurately with a low computational cost. Useful formulas for evaluating matrix elements with the CG-GV basis are collected in appendices of Refs. [37,38].

C. Basis functions for electric dipole excitation

We construct basis functions for the final states with $J^\pi = 1^-$ that are excited by the $E1$ operator

$$\mathcal{M}_{1\mu} = e\sum_{i\in p}(\boldsymbol{r}_i - \boldsymbol{x}_6)_\mu = \sqrt{\frac{4\pi}{3}}e\sum_{i\in p}\mathcal{Y}_{1\mu}(\boldsymbol{r}_i - \boldsymbol{x}_6), \quad (6)$$

where the summation runs over protons, and $\boldsymbol{x}_6$ is the c.m. coordinate of ^{6}He. We apply the same prescription as that of Refs. [39,40] adopted for the study of $E1$ and spin-dipole strength in $N = 4$ system to the six-body calculation of $E1$ strength. In that study four-body continuum-discretized states are constructed by taking into account both sum rules and final state interactions, and thereby the model reproduces experimental data satisfactorily and in addition leads to some predictions. The configurations that we include here are (i) the sp excitation built with $\mathcal{Y}_{1\mu}(\boldsymbol{r}_1 - \boldsymbol{x}_6)$, (ii) the $\alpha + n + n$ three-body decay channel, and (iii) the $t + d + n$ three-body decay channel. Figure 1 illustrates schematic diagrams of the above three configurations for the $E1$ excitation of ^{6}He. Because of a Borromean nature of ^{6}He, an explicit inclusion of the three-body final states is important. The basis (i) is vital to satisfy the sum rule, and the bases (ii) and (iii) take care of final state interactions in the three-body decay asymptotics.

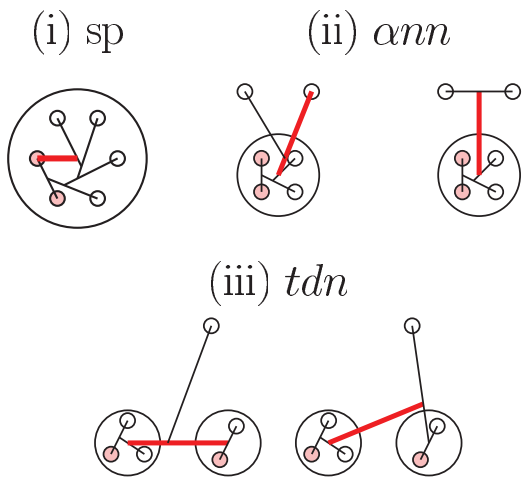

FIG. 1. (Color online) Schematic diagrams of three patterns for the $E1$ excitations of ^{6}He. Small circles and shaded ones denote neutron and proton, respectively. Thick solid lines denote the coordinates on which the $E1$ operator acts.

The detail of each configuration is given below. It should be noted, however, that the three classes of configurations are not orthogonal to each other but have considerable overlap among others.

1. Single-particle excitation

We define the sp basis by

$$\Psi^{\rm sp}_f = \mathcal{A}\big[\Phi^{(6)}_{0,i}\mathcal{Y}_1(\boldsymbol{r}_1-\boldsymbol{x}_6)\big]_{1\mu}, \tag{7}$$

where $\Phi^{(6)}_{0,i}$ is the ith component of the ground state wave function of ^{6}He. The basis state describes a sp excitation from the ground state by the $E1$ operator and plays an important role in accounting for the $E1$ sum rule. If $\Phi^{(6)}_{0,i}$ is replaced with the ground state wave function of ^{6}He, $\Psi^{\rm sp}_f$ reduces to the coherent state that exhausts all the $E1$ strength reached from the ground state. Since all the components are included independently in the present calculation, the set of the basis functions takes into account the effect of the pseudoexcited 0^+ states of ^{6}He.

2. α + n + n three-body decay channel

The $\alpha+n+n$ channel is the lowest threshold of ^{6}He and is expected to be important to describe the SDM. We explicitly include the $\alpha+n+n$ configurations in the form

$$\Psi^{\alpha nn}_f = \mathcal{A}\big[\Phi^{(4)}_{0,i}\exp\left(-\tfrac{1}{2}\tilde{\boldsymbol{y}}B\boldsymbol{y}\right)\big[\mathcal{Y}_1(\tilde{w}\boldsymbol{y})\chi^{(2)}_{S_{56}}\big]_1\big]_{1\mu}, \tag{8}$$

where $\Phi^{(4)}_{0,i}$ is the ith basis state of the ground state wave function of ^{4}He, and $\tilde{\boldsymbol{y}}=(\boldsymbol{y}_1\,\boldsymbol{y}_2)$ where the coordinates $\boldsymbol{y}_1$ and $\boldsymbol{y}_2$ specify the three-body character of $\alpha+n+n$ and so-called Y- and T-type coordinates are both employed. Further detail is given in the next paragraph [see Fig. 1(ii)]. A 2×2 positive-definite, symmetric matrix B that characterizes a spatial configuration of the two valence neutrons is chosen to cover the physically important region for describing weakly bound two neutrons. A choice of w is also explained below. The spin of the two neutrons, S_{56}, can be 0 and 1, and both are included independently in the basis set. The isospin functions are not written explicitly in Eq. (8) for the sake of simplicity. In order to reduce a computational cost, we prepare a truncated ^{4}He wave function with 15 basis states, which leads to an energy loss of 0.3 MeV. We also calculate the $E1$ strength with 20 and 25 basis states and confirm that no qualitative difference is obtained in the $E1$ strength below 20 MeV excitation energy where the α core remains in its ground state. Since the basis state $\Phi^{(4)}_{0,i}$ is included independently, the two neutrons are allowed to move against the α core in its pseudoexcited state.

Both Y- and T-type coordinates are defined by

$$\begin{aligned}
&\boldsymbol{y}^{(\rm Y)}:\ \boldsymbol{y}^{(\rm Y)}_1=\boldsymbol{r}_5-\boldsymbol{x}^{(4)}_{\rm cm},\quad \boldsymbol{y}^{(\rm Y)}_2=\boldsymbol{r}_6-\frac{\boldsymbol{r}_5+4\boldsymbol{x}^{(4)}_{\rm cm}}{5},\\
&\boldsymbol{y}^{(\rm T)}:\ \boldsymbol{y}^{(\rm T)}_1=\boldsymbol{r}_6-\boldsymbol{r}_5,\quad \boldsymbol{y}^{(\rm T)}_2=\frac{\boldsymbol{r}_5+\boldsymbol{r}_6}{2}-\boldsymbol{x}^{(4)}_{\rm cm},
\end{aligned} \tag{9}$$

where $\boldsymbol{x}^{(N)}_{\rm cm}$ denotes the c.m. coordinate of an N-particle system. Since the main neutron configuration in the ground state of ^{6}He is $(0s)^2(0p)^2$, the $E1$ operator acting on the halo neutron changes one of the P orbits to an extended S orbit in the continuum. In the case of Y type that describes a valence-neutron excitation the S wave is assigned to $\boldsymbol{y}^{(\rm Y)}_1$ and the remaining P wave to $\boldsymbol{y}^{(\rm Y)}_2$. In the case of T type that is very important to describe the SDM-like excitation the S wave is assigned to $\boldsymbol{y}^{(\rm T)}_1$ while the P wave to $\boldsymbol{y}^{(\rm T)}_2$. The above assignment of the partial waves can be made possible by choosing $\tilde{w}=(0\,1)$ and B to be diagonal.

In practical calculations, first we generate the diagonal matrix elements of B, and then transform the coordinates $\boldsymbol{y}^{(\rm Y)}$ or $\boldsymbol{y}^{(\rm T)}$ together with three coordinates used to describe $\Phi^{(4)}_{0,i}$ to the $\boldsymbol{x}$ coordinate. This transformation is carried out by an appropriate matrix T. Substitution of $\boldsymbol{y}=T\boldsymbol{x}$ into Eq. (8) reduces the $\alpha+n+n$ configurations to the standard CG-GV basis function of Eq. (2). The diagonal elements, B_{11} and B_{22}, are taken by a geometrical progression with different Gaussian falloff parameters ranging from 0.1 to 22 fm: More explicitly, they are chosen as $B_{11}=(0.13\times 1.35^{(n-1)})^{-2}$ $(n=1,\ldots 18)$ and $B_{22}=(0.2\times 1.4^{(m-1)})^{-2}$ $(m=1,\ldots 15)$ in both Y and T types.

3. t + d + n three-body decay channel

We here treat the $t+d+n$ three-body decay channel. This channel is important to describe the $E1$ strength especially in the GDR region because it involves the excitation of the α core. The channel is the third lowest threshold of ^{6}He and makes it possible to describe those configurations in which two protons, excited by the $E1$ operator, are apart from each other. With the coordinate sets appropriate for describing the three-body system,

$$\begin{aligned}
&\boldsymbol{z}^{(\rm Y)}:\ \boldsymbol{z}^{(\rm Y)}_1=\boldsymbol{x}^{(2)}_{\rm cm}-\boldsymbol{x}^{(3)}_{\rm cm},\quad \boldsymbol{z}^{(\rm Y)}_2=\boldsymbol{r}_6-\frac{2\boldsymbol{x}^{(2)}_{\rm cm}+3\boldsymbol{x}^{(3)}_{\rm cm}}{5},\\
&\boldsymbol{z}^{(\rm T)}:\ \boldsymbol{z}^{(\rm T)}_1=\frac{\boldsymbol{r}_6+2\boldsymbol{x}^{(2)}_{\rm cm}}{3}-\boldsymbol{x}^{(3)}_{\rm cm},\quad \boldsymbol{z}^{(\rm T)}_2=\boldsymbol{r}_6-\boldsymbol{x}^{(2)}_{\rm cm},
\end{aligned} \tag{10}$$

the basis functions are expressed as

$$\Psi_f^{tdn} = \mathcal{A}\Big[\Big[\Phi^{(3)}_{1/2,i}\Phi^{(2)}_{1,j}\Big]_{J_{12}} \times \exp\Big(-\tfrac{1}{2}\tilde{z}Bz\Big)\Big[\mathcal{Y}_1(\tilde{w}z)\Phi^{(1)}_{1/2}\Big]_{J_{34}}\Big]_{1\mu}, \quad (11)$$

where $\tilde{z} = (z_1\, z_2)$, and $\Phi^{(3)}_{1/2,i}$ and $\Phi^{(2)}_{1,j}$ are ith and jth basis functions of ^{3}H and ^{2}H, respectively. They are approximated by 7 for ^{3}H and 3 basis states for ^{2}H. The $\Phi^{(1)}_{1/2}$ represents the single neutron spin and isospin function. The intermediate spins, J_{12} and J_{34}, take 1/2 and 3/2, and they are included independently. The partial wave of the first relative coordinate in each coordinate set is chosen to be a P wave that is excited by the $E1$ operator. The basis states take into account the asymptotics of the three-body decay due to the $E1$ excitation as well as a coupling with the pseudostates of ^{3}H and ^{2}H. Similarly to the construction of $\alpha + n + n$ basis states, we set $\tilde{w} = (1\,0)$ and choose the diagonal matrix element of B as $B_{11} = (0.7 \times 2.0^{(n-1)})^{-2}$ $(n = 1, \ldots, 5)$ and $B_{22} = (0.7 \times 2.0^{(m-1)})^{-2}$ $(m = 1, \ldots, 5)$.

Note that the $t + t$ two-body decay channel, the second lowest threshold of ^{6}He, does not contribute to the $E1$ strength in the present model. The $t + t$ channel with the relative P-wave motion has to have $S = 1$ and $T = 1$. Since the ground state of ^{6}He is described with the $S = 0$ configurations and the $E1$ operator does not change the spin, any $t + t$ configurations with $S = 1$ cannot be excited by $E1$. If a realistic nuclear force is used, both $S = 0$ and $S = 1$ configurations couple and the $t + t$ channel gives some contribution to the $E1$ strength.

The number of basis functions in each diagram is 600 for sp, 4050 × 2 for $\alpha + n + n$, and 2625 × 2 for $t + d + n$. The calculation is performed not only in each basis set but also in a "full" model space that combines all of them. The total number of basis functions in the full calculation is 13 950. Since all $E1$ strength of ^{6}He exists in the continuum above the $\alpha + n + n$ threshold, our calculation is practically an approximation with the continuum discretization. Because of the extensive basis states, however, the number of discretized states is so dense that on average ten states appear per 1 MeV below the excitation energy of 50 MeV.

III. RESULTS AND DISCUSSIONS

A. Ground state properties

The CG-GV basis with the SVM optimization gives an efficient description of the ground state of ^{6}He. Figure 2 displays the convergent curve of the ground state energy of ^{6}He calculated with $u = 1.0$ of the MN potential. We increase the number of basis functions competitively according to the algorithm of the SVM [26,35]. A sudden decrease of the energy at the 300th basis state is due to the SVM refinement procedure in which the basis dimension is fixed but each basis function is compared with the best one among randomly generated candidates. The converged energy is obtained only with 600 basis states, which is surprisingly small if one recalls that each basis function has 15 variational parameters for the orbital part (4). No decrease of the energy is obtained when we make the refinement of the 600 basis states. The calculated ground state energy of ^{6}He with $u = 1.0$ is consistent with that obtained by the calculation of the 600 dimension in Ref. [26]. In fact it is 0.25 MeV lower than that because of the improvement of the asymptotics of the wave function. The root mean square (rms) matter radius, r_m, is found to be larger by 0.08 fm than that of Ref. [26].

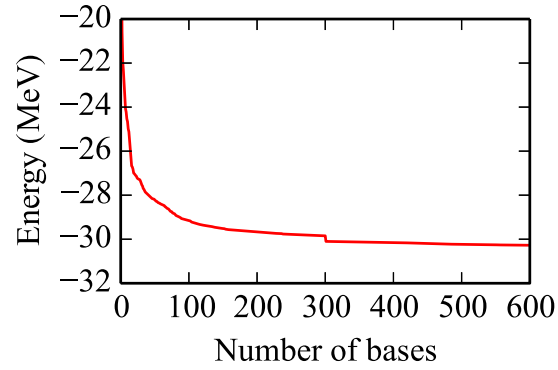

FIG. 2. (Color online) Energy convergence of ^{6}He as a function of basis dimension. The parameter u of the MN potential is set to be unity.

Calculated physical quantities are summarized in Table I for different u values. Our results on binding energies are also consistent with those by EIHH [42] for all u values. Since the u parameter controls the strength of the odd-partial waves, the binding energy and radius of ^{4}He, which has almost $(0s_{1/2})^4$ configuration, do not depend on u. Some dependence on u appears for ^{6}He, however, because the two valence neutrons move in the P orbit according to the simplest shell model. A larger u value gives a more attractive P-wave interaction. It is found that the experimental S_{2n} value is reproduced with $u = 1.05$, so that we use $u = 1.05$ in what follows unless otherwise mentioned.

Our wave function for ^{4}He underestimates its point proton rms radius r_p by 0.05 fm [43], and partly because of this the calculated r_p of ^{6}He is slightly smaller than the experimental values, 1.938(23) [44] and 1.912(18) [45], extracted from charge radius measurements. The experimental matter radius

TABLE I. Energy, two-neutron separation energy, and rms radii of of ^{4}He and ^{6}He. See text for details. Energy and length are given in units of MeV and fm, respectively. Experimental data are taken from Ref. [41].

		u					Expt.
		1.00	1.05	1.10	1.20	1.30	
E	^{6}He	−30.32	−30.98	−31.71	−33.45	−35.53	−29.27
S_{2n}	^{6}He	0.39	1.01	1.72	3.39	5.41	0.972
r_m	^{6}He	2.52	2.41	2.32	2.16	2.05	
	^{4}He	1.41	1.41	1.41	1.41	1.41	
r_p	^{6}He	1.90	1.83	1.78	1.68	1.61	
	^{4}He	1.41	1.41	1.41	1.41	1.41	
r_n	^{6}He	2.78	2.65	2.54	2.37	2.23	
	^{4}He	1.41	1.41	1.41	1.41	1.41	
r_{pp}	^{6}He	2.50	2.49	2.48	2.44	2.39	
	^{4}He	2.37	2.37	2.37	2.37	2.37	

of ^{6}He is not as precise as the proton radius and is somewhat scattered: The empirical values are 2.48(3) [3], 2.30(7) [46], 2.33(4) [47], and 2.37(5) [48]. The averaged empirical matter radius, 2.37(10) fm, is consistent with the calculated matter radius. Many theoretical works have been devoted to understanding the rms radii of ^{6}He with different methods and interactions. See, e.g., Ref. [44,49] and references therein.

The r_p value of ^{6}He is not necessarily the same as that of ^{4}He due to a recoil effect of the core. Even though the $\alpha+n+n$ three-body model is quite good for the ground state of ^{6}He, the r_p value of ^{6}He becomes larger than that of ^{4}He because the c.m. of the α core moves around the c.m. of ^{6}He, and the difference between them depends on the extent to which the c.m. of the α core fluctuates. Denoting the relative distance vector between the core and the c.m. of the two valence neutrons by $\boldsymbol{R}=\boldsymbol{y}_2^{(\mathrm{T})}$, in general we obtain the following relation between the r_p values of A and $A-2$ systems [16,50],

$$\langle r_p^2(A)\rangle = \langle r_p^2(A-2)\rangle + \frac{4}{A^2}\langle \boldsymbol{R}^2\rangle. \tag{12}$$

The second term on the right-hand side of the above equation expresses the recoil effect. With Eq. (12), the expectation value of the relative distance, $\sqrt{\langle R^2\rangle}$, is estimated as 3.50 fm, which is consistent with 3.89 fm obtained by an $\alpha+n+n$ three-body calculation [50].

The rms distance of the two protons, r_{pp}, serves as a measure of whether the ^{4}He core is frozen or not in ^{6}He. If the two-proton configuration of ^{6}He is the same as that of ^{4}He, their r_{pp} values are expected to be the same. The r_{pp} of ^{6}He is found to be 5% larger than that of ^{4}He, which indicates a core swelling. This effect becomes larger as the valence neutron binding energy decreases. As pointed out in Ref. [22], the proton tail of the α core plays a vital role in binding the two valence neutrons. A proton tends to be closer to neutrons rather than to the other proton because the pn interaction is stronger than the pp interaction. In the case that the valence neutrons are weakly bound, the proton in the α core is attracted by the valence neutrons moving far from the core, and thus r_{pp} of ^{6}He becomes larger than that of the free α particle. The effect is never taken into account in a macroscopic three-body model of $\alpha+n+n$ but is realized in a fully microscopic six-body model.

Figure 3 displays the density distributions of ^{4,6}He defined by

$$\rho_{p/n}(r) = \langle\Psi_0|\sum_{i\in p/n}\delta\left(\left|\boldsymbol{r}_i-\boldsymbol{x}_{\mathrm{cm}}^{(N)}\right|-r\right)|\Psi_0\rangle, \tag{13}$$

where Ψ_0 is the ground state wave function. The density is normalized to the number of protons or neutrons. The density distributions for both proton and neutron are the same in ^{4}He and their peak position is 1.1 fm, whereas the neutron density of ^{6}He, peaked at 1.7 fm, is very much extended showing a two-neutron halo feature. The peak of the proton density of ^{6}He is shifted to 1.3 fm due to the recoil effect, and the density exhibits more extended distribution than that of ^{4}He.

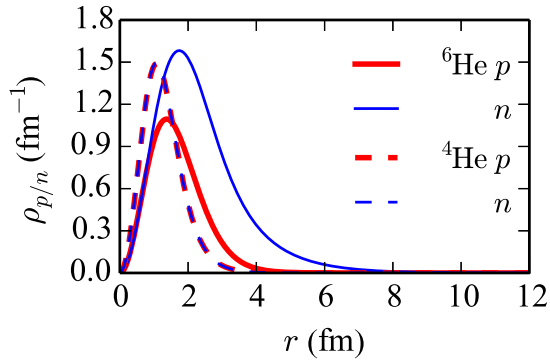

FIG. 3. (Color online) Proton and neutron density distributions of ^{4,6}He.

B. Electric dipole strength

We show continuum-discretized $E1$ strength. The Hamiltonian is diagonalized in the basis states that are defined in Sec. II C, and the reduced transition probability for the $E1$ operator is calculated by

$$B(E1,\nu) = \sum_{M\mu}|\langle\,\Psi_{1M}(E_\nu)|\mathcal{M}_{1\mu}|\Psi_0\,\rangle|^2\,, \tag{14}$$

where $\Psi_{1M}(E_\nu)$ is νth final state wave function with excitation energy E_ν.

Figure 4 displays the $E1$ strength calculated with each model space as well as with the full space. The sp model space produces two prominent and concentrated peaks at 6.91 and 13.20 MeV and fragmented strength at the excitation energy of 30–40 MeV. The two prominent peaks may correspond to the observed levels at 5.6 and 14.6 MeV with large decay widths, 12.1 and 7.4 MeV, respectively [51], though their J^π values are not identified as 1^-. The fragmented strength at the higher energy region appears to correspond to the GDR. Compared to the sp result, the $\alpha+n+n$ model space presents many much smaller and fragmented peaks due to the weak binding nature of the valence neutrons. Small peaks are concentrated at the low-energy region around 4 MeV. These peaks in the low-lying $E1$ strength may correspond to the SDM. The $t+d+n$ model space presents several concentrated peaks below 24 MeV as well as many fragmented strength beyond that energy. As discussed before, this model space explicitly includes the configurations in which two protons can be apart from each other, and we will confirm later that this class of model space plays a decisive role in describing the GDR due to the core excitations.

We study the mechanism of the appearance of the low-lying $E1$ strength and note that the SDM discussed here does not necessarily mean a narrow resonance. A microscopic $\alpha+n+n$ cluster model calculation was performed in Ref. [52] to find low-lying 1^- resonances with the complex scaling method, and no such resonant state appeared in the low-energy region. As seen in Fig. 4(a), the strength distribution in the low-energy region is densely obtained but no such peak is found that is sufficiently stable against the increase of the model space. It is unlikely to obtain a narrow low-lying 1^- resonance consistently with the result of Ref. [52].

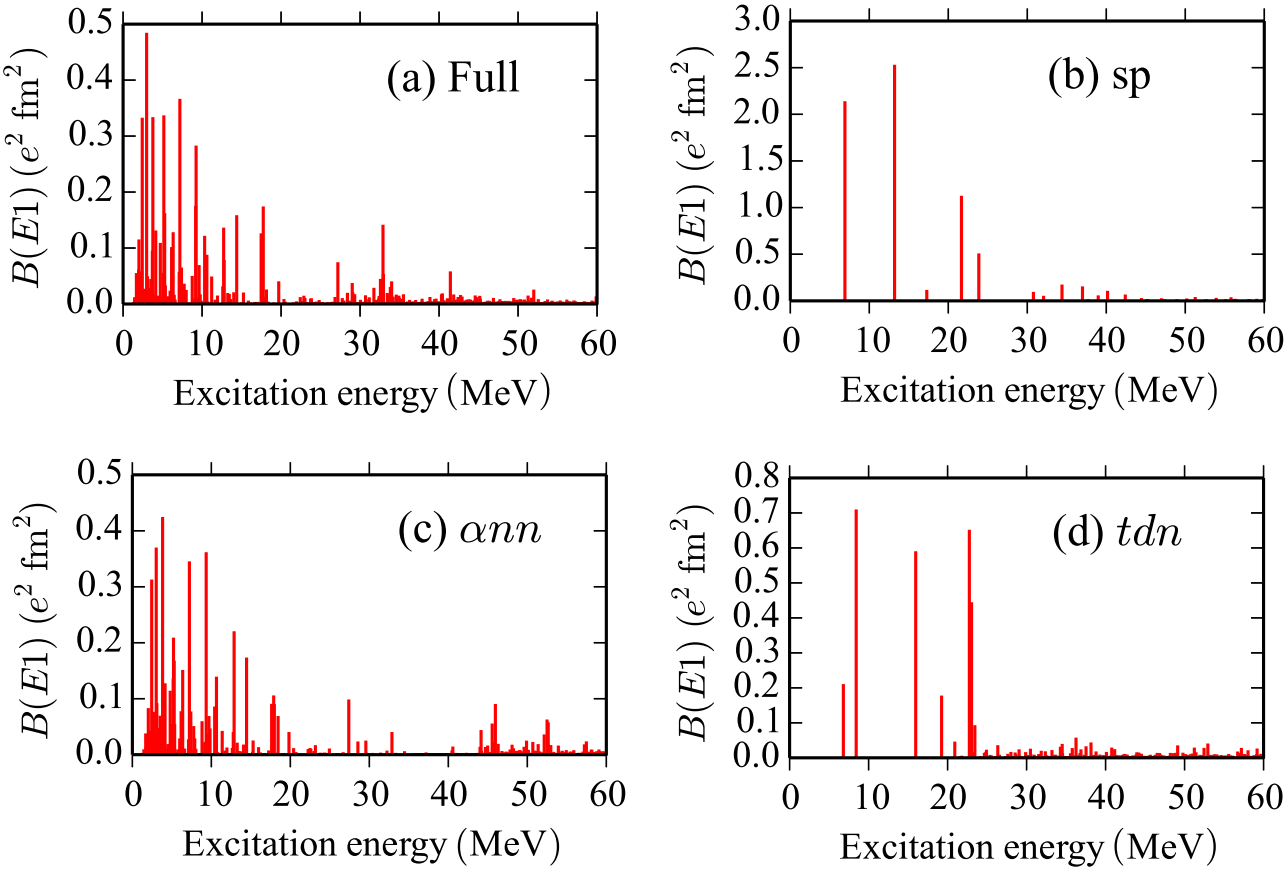

FIG. 4. (Color online) Electric dipole strength of ^{6}He calculated with each basis set of the excitation diagram. Full indicates the result of calculation including all the basis sets. Note the different scale of the sp $B(E1)$ value.

As noted already, each model space has significant overlap, and in the calculation of the full model space almost all the prominent peaks are fragmented into small strength. Roughly speaking, the strength distribution can be divided into two groups: broad and strong low-lying strength centered around 3 MeV and extending to 20 MeV and higher peaks at 33 MeV. It is apparent that the $\alpha + n + n$ configurations are of vital importance in describing the low-lying $E1$ strength because the low-lying peaks show up only with the $\alpha + n + n$ configurations. It should be noted, however, that the full model enhances the low-lying $E1$ strength below about 5 MeV more strongly than the $\alpha + n + n$ model. The strength at around 33 MeV corresponds to the GDR and apparently appears when the core excited configurations are explicitly included.

What is the possible structure of the GDR in ^{6}He? Since the GDR regions already exceed the breakup threshold of ^{4}He, the breaking of the α core should play an essential role. Figure 5 displays the $E1$ strength for ^{4}He. The excited 1^- states are constructed as in Ref. [39]. Differently from ^{6}He, no strength appears at the low-energy region because the threshold of $^3\mathrm{H} + p$ is fairly high. Four prominent peaks are found at 25.0, 27.5, 31.8, and 39.9 MeV, and we see that several peaks in ^{6}He appear at the positions similar to those energies. We will confirm in Sec. III E that the peaks in the region between 33 and 41 MeV are due to the excitation of the α core.

The $E1$ sum rule is useful as a qualitative measure of judging the extent to which the model space is extensive to describe the $E1$ excitation. If $\Psi_{1M}(E_\nu)$ of Eq. (14) forms a complete set for configurations with 1^-, a well-known non-energy-weighted sum rule for the $E1$ operator reads

$$\sum_\nu B(E1,\nu) = e^2\left(Z^2\langle r_p^2\rangle - \frac{Z(Z-1)}{2}\langle r_{pp}^2\rangle\right), \qquad (15)$$

where Z is the number of protons. The right-hand side of the above equation depends only on the ground state properties, which turns out to be 7.21 e^2 fm^2. We obtain 99.8, 90.4, and

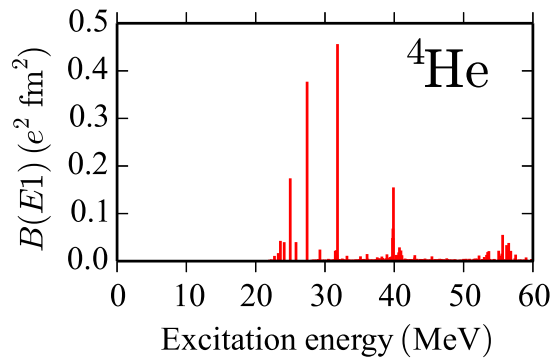

FIG. 5. (Color online) Electric dipole strength of ^{4}He.

65.8% of the sum rule for the sp, $\alpha+n+n$, and $t+d+n$ configurations, respectively. The full space exhausts 99.9% of the sum rule. This confirms that our model space is extensive enough to account for the configurations excited by the $E1$ operator. It should be noted, however, that the sp model space alone accounts for the sum rule but the fragmentation of the $E1$ strength is possible only with the coupling to the $\alpha+n+n$ and $t+d+n$ model space.

C. Comparison with experiment

The $E1$ strength function is approximately obtained by a convolution of $B(E1)$ with the Lorentzian function as follows:

$$\frac{dB(E1,E)}{dE} = \sum_{\nu} N(E_\nu,\Gamma)L(E,E_\nu,\Gamma)B(E1,\nu) \quad (16)$$

with

$$L(E,E_\nu,\Gamma) = \frac{\Gamma}{2\pi}\frac{1}{(E-E_\nu)^2+(\Gamma/2)^2}, \quad (17)$$

$$N(E_\nu,\Gamma) = \frac{1}{1-\int_{-\infty}^{E_{\rm th}} L(E',E_\nu,\Gamma)dE'}, \quad (18)$$

where $N(E_\nu,\Gamma)$ is introduced to renormalize the strength near the two-neutron threshold of ^{6}He, $E_{\rm th}$, satisfying $N(E_\nu,\Gamma)\int_{E_{\rm th}}^{\infty} L(E,E_\nu,\Gamma)dE = 1$. Figure 6 compares the calculated $E1$ strength function with that extracted from the Coulomb breakup measurement [5]. The hatched band indicates the variation of theoretical strength functions for different width parameters, $\Gamma = 0.75$ to 2.0 MeV. The range of Γ is chosen referring to Ref. [21]. An oscillatory behavior of the $E1$ strength is observed with the small Γ but the Γ dependence becomes small for $\Gamma > 1$ MeV. In view of large error bars of the data we conclude that the calculated $E1$ strength function fairly well agrees with experiment.

Figure 7 displays the $E1$ strength function in wider energy range. The width Γ is taken as 2.0 MeV. The peak at the lower energy is expected to have the SDM structure while the other has the GDR structure as implied by Ref. [23]. We examine the sensitivity of the $E1$ strength function to the u parameter. The peak position at the low excitation energy shifts drastically to higher energy and its strength becomes much smaller with increasing u. This is easily understood because the valence neutrons get more binding and are not easily excited (see Table I). No drastic change of the peak position and strength is found in the GDR region around 33 MeV where the α breaking is dominant. As confirmed above, the large enhancement of the $E1$ strength at low energy is due to the weakly bound neutrons, and therefore reproducing the experimental two-neutron separation energy is essential to account for the low-lying $E1$ strength. We obtain some other peaks at 10 and 18 MeV as seen in Fig. 7. We will discuss their structure in Sec. III D.

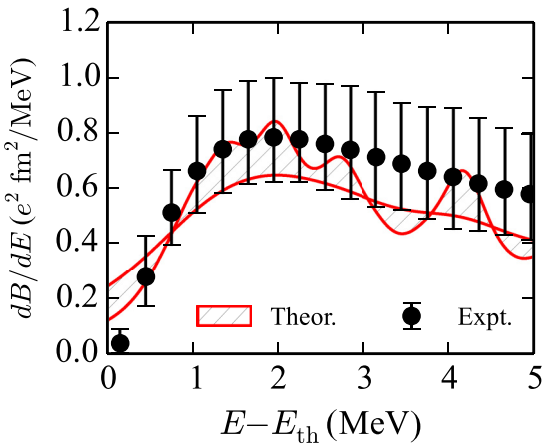

FIG. 6. (Color online) Electric dipole strength functions of ^{6}He measured from the threshold energy $E_{\rm th}$. A hatched area denotes theoretical uncertainly due to a choice of the smearing width ranging from 0.75 to 2.0 MeV in the Lorentzian function (18). Experimental data taken from Ref. [5] are multiplied by $\frac{4\pi}{3}$ to be consistently with the $E1$ operator of Eq. (6).

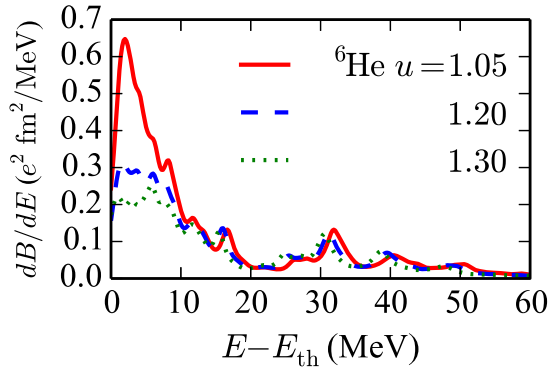

FIG. 7. (Color online) The same as Fig. 6 but for a wider energy region. The results with different u parameters of the MN potential are also plotted. The smearing width of the Lorentzian function is set to be 2.0 MeV.

D. Soft and giant dipole excitation modes

To discuss how the protons and neutrons respond in the $E1$ excitation, we calculate the $E1$ transition density,

$$\rho^{\rm tr}_{p/n}(E_\nu,r) = \langle\Psi_1(E_\nu)\|\sum_{i\in p/n}\mathcal{Y}_1(\boldsymbol{r}_i-\boldsymbol{x}_6) \times\delta(|\boldsymbol{r}_i-\boldsymbol{x}_6|-r)\|\Psi_0\rangle. \quad (19)$$

As defined in Eq. (6), the $E1$ transition matrix element is given by the proton transition density as

$$\langle\Psi_1(E_\nu)\|\mathcal{M}_1\|\Psi_0\rangle = e\sqrt{\frac{4\pi}{3}}\int_0^\infty \rho^{\rm tr}_p(E_\nu,r)dr. \quad (20)$$

If the $\alpha+n+n$ three-body model is assumed and no excitation of the α core is allowed, the neutron transition density is related to the proton transition density by

$$\rho^{\rm tr}_n(E_\nu,r) = \rho^{\rm tr}_p(E_\nu,r) + \rho^{\rm tr}_{2n}(E_\nu,r), \quad (21)$$

where $\rho^{\rm tr}_{2n}(E_\nu,r)$ stands for a contribution from the halo neutrons and it is entirely determined by the two-neutron wave function.

Figure 8 plots the proton and neutron transition densities of the most prominent peaks at about 3, 7, 18, and 33 MeV. In

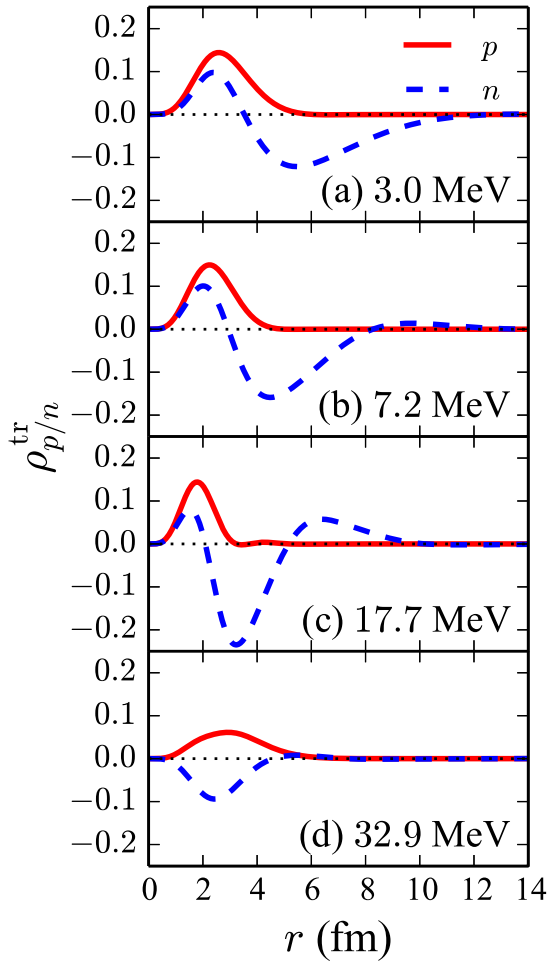

FIG. 8. (Color online) Electric dipole transition densities for proton and neutron of the states with the excitation energy of (a) 3.0, (b) 7.2, (c) 17.7, and (d) 32.9 MeV, respectively.

the lowest prominent peak at 3.0 MeV, the transition densities of proton and neutron coincide up to about 1.7 fm, which corresponds to the peak of the ground state neutron density (see Fig. 3). The neutron transition density deviates from the proton one beyond 1.7 fm, showing in-phase oscillation in the interior region, $r \lesssim 3$ fm, and out-of-phase oscillation in the external region $r \gtrsim 3$ fm. Furthermore, the neutron transition density is very much extended beyond 10 fm. These observations agree with what we expect from the relationship (21) for an ideal SDM and are consistent with the classical interpretation of the SDM discussed in Ref. [10]. As the energy increases up to 18 MeV, the proton transition density gradually shrinks but its basic pattern is still kept. This shrinkage is due to the fact that the $\rho^{\rm tr}_{2n}(E_\nu, r)$ of the neutron transition density vibrates more and more rapidly with an increase of the number of nodes of oscillation. Though the penetration of the valence neutrons into the internal region grows gradually, the internal structure characteristic of the SDM does not change so much as shown in Figs. 8(b) and 8(c). The oscillatory behavior becomes even stronger at 17.7 MeV, showing little distortion of the core. The neutron transition density reaches a maximum at 3.4 fm. The protons follow the motion of the neutrons, and the resulting

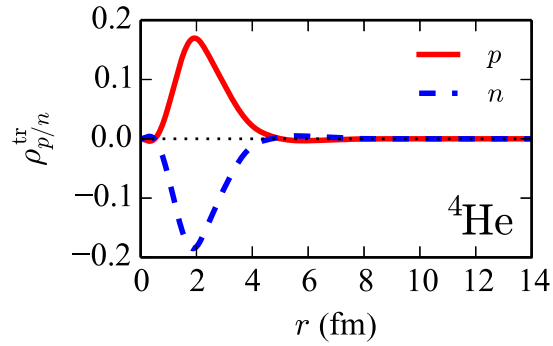

FIG. 9. (Color online) Electric dipole transition densities for proton and neutron of ^{4}He at the excitation energy of 31.8 MeV.

proton transition density exhibits a destructive pattern. Such neutron oscillation leads to the smaller $E1$ strength than that of the lowest-lying peak.

At the higher peak with 33 MeV, the transition densities clearly show the out-of-phase oscillation in the whole region, which is typical of the GDR. The proton transition density shows somewhat broader distribution than those of the low-lying states. This suggests the strong distortion of the core due to the dipole field, which can never be described by $\alpha + n + n$ three-body models with an inert core. As an example of the ideal GDR, we plot in Fig. 9 the transition densities of the most prominent strength of ^{4}He at 31.8 MeV (see Fig. 5). Both the proton and neutron transition densities show the identical distribution with opposite phases. They are peaked at 1.9 fm, which is further inside than those of the GDR of ^{6}He.

We also investigate the excited modes of ^{6}He at about 40 MeV and find that their transition densities are similar to that of the GDR but have more oscillations and smaller amplitudes.

E. Validity of $\alpha + n + n$ three-body picture

To examine how good the three-body model of $\alpha + n + n$ is for ^{6}He, we study the cluster sum rule [53] as a qualitative measure. We rewrite the $E1$ operator (6) as

$$\mathcal{M}_{1\mu} = e\left(\sum_{i\in p}\left(\boldsymbol{r}_i - \boldsymbol{x}^{(A-2)}_{\rm cm}\right)_\mu - \frac{2Z}{A}\boldsymbol{R}_\mu\right). \qquad (22)$$

If the system has a core plus two-nucleon structure and the first term on the right-hand side of the above equation does not contribute to the $E1$ strength, we obtain the non-energy-weighted cluster sum rule [54,55]:

$$B(E1;\mathrm{NEWCSR}) = e^2\left(\frac{2Z}{A}\right)^2\langle \boldsymbol{R}^2\rangle. \qquad (23)$$

We calculate a cumulative sum of the $E1$ strength, $\sum_{\nu=1}^{\nu_{\max}} B(E1,\nu)$, and find that the cumulative sum exceeds the $B(E1;\mathrm{NEWCSR})$ value of 5.44 e^2 fm^2 at $E_{\nu_{\max}} = 26.8$ MeV. Therefore the cluster sum rule occupies about 75% of the non-energy-weighted sum rule (15) and its strength appears below the excitation energy of 25 MeV. Since the GDR appears

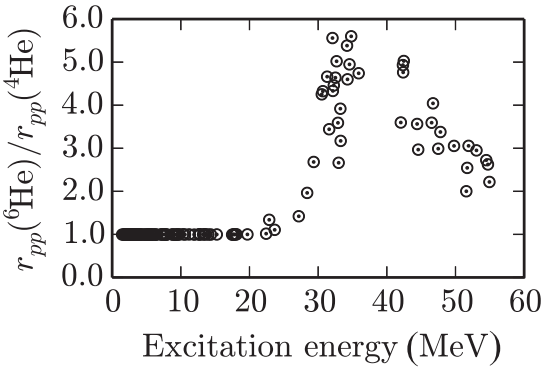

FIG. 10. Ratio of the proton-proton (pp) distance of ^{6}He to that of the ground state of ^{4}He as a function of $E1$ excitation energy.

above 30 MeV, we conclude that the SDM and GDR are well separated and the low-lying strength is understood with the $\alpha + n + n$ three-body structure.

The above conclusion is further confirmed by calculating the proton-proton rms distance, r_{pp}, of the state $\Psi_{1M}(E_v)$ because r_{pp} can be a measure of whether or not the α core exists in ^{6}He. By selecting those states that have $1/1000$ of the $E1$ sum rule value, we plot in Fig. 10 the ratio of r_{pp} of ^{6}He to that of ^{4}He. The ratio is unity up to the excitation energy of about 20 MeV that corresponds to the excitation energy of the first excited 0^+ state of ^{4}He (20.21 MeV [56]). This indicates that the core is not virtually excited, and thus the three-body picture holds very well in the low-energy region below 20 MeV. As discussed in Sec. III A, the ground state of ^{6}He has 5% larger r_{pp} than that of ^{4}He. No such core swelling effect is found, however, in the low-lying 1^- states. In the 1^- states the valence neutrons are further away from the core and receive essentially no interaction from the core. Beyond the excitation energy of 20 MeV, the ratio suddenly increases and reaches a maximum at the GDR region, indicating a large distortion of the core.

In Ref. [23] the two-peak structure of the $E1$ strength function of ^{6}He is discussed from the isospin decomposition to $T = 1$ and 2 states. The low-lying peak is dominated by the total isospin $T = 1$ state, and above $\sim$20 MeV the $T = 2$ component contributes as well. Since the three-body structure of $\alpha + n + n$ consists of $T = 1$, our finding in the r_{pp} analysis is consistent with the result of Ref. [23].

The core excitation often plays an important role in enhancing the low-lying $E1$ strength of two-neutron halo nuclei. For example, in the case of ^{11}Li, core excitations produce a large admixture of the $(1s_{1/2})^2$ component in the ground state [57–59]. Such very extended S orbitals enhance the matter radius as well as the low-lying $E1$ strength [59,60]. In Ref. [61], the $E1$ strength function of ^{22}C is discussed with the Skyrme-Hartree-Fock method on a three-dimensional coordinate space and the core (^{20}C) excitation is found to play an important role to account for the $E1$ strength. The transition densities for the PDR and GDR regions shown in the paper are similar to those obtained in the present work. There is however a clear difference between ^{22}C and ^{6}He. In the case of ^{22}C the single-particle energies of the $0d_{5/2}$ and $1s_{1/2}$ orbitals are very close, and the nucleons in the $0d_{5/2}$ orbits can easily be excited to continuum by the $E1$ operator, which is a dominant process of the core excitation in the low-energy region. In the case of ^{6}He, however, the α core is not easily excited and the energy gap between the $0s_{1/2}$ and $0p_{3/2}$ orbitals is fairly large. As a result of both effects the motion of the core and valence neutrons decouples approximately in the low-lying $E1$ excitation.

The large enhancement of the low-lying $E1$ transition in the two-neutron halo nuclei is mainly due to the weak binding feature of the valence nucleons, but a special care about the structure of the core is needed for understanding its origin.

F. Compressional $E1$ mode

We examine another $E1$ mode, the so-called compressional $E1$ ($cE1$) mode [62]. The operator for the mode is defined as

$$\mathcal{M}^{\mathrm{comp.}}_{1\mu} = e \sum_{i\in p} |\boldsymbol{r}_i - \boldsymbol{x}_6|^3 Y_{1\mu}(\widehat{\boldsymbol{r}_i - \boldsymbol{x}_6}). \tag{24}$$

According to a simple harmonic-oscillator shell model, the $cE1$ mode appears at the high-energy region because it requires at least $3\hbar\omega$ excitations from the $0\hbar\omega$ ground state. However, if the ground state contains some amount of correlated components, the mode may appear at the low-energy region by coupling with higher oscillator shells that are already incorporated in the ground state wave function. The matrix element of $\mathcal{M}^{\mathrm{comp.}}_{1\mu}$ is given by the proton transition density as

$$\langle \Psi_1(E_v) \| \mathcal{M}^{\mathrm{comp.}}_1 \| \Psi_0 \rangle = e \int_0^\infty r^2 \rho^{\mathrm{tr}}_p(E_v, r) dr. \tag{25}$$

The matrix element for the isoscalar (IS) compressional dipole ($c1$) mode is calculated as

$$\int_0^\infty r^2 \big(\rho^{\mathrm{tr}}_p(E_v, r) + \rho^{\mathrm{tr}}_n(E_v, r)\big) dr. \tag{26}$$

Since the transition is not necessarily induced by the electromagnetic interaction but the nuclear one, we omit e from the matrix element.

Figure 11 displays the $cE1$ strengths as a function of the excitation energy. Similarly to the normal $E1$ operator, the two-peak structure is found but the low-lying peaks are more

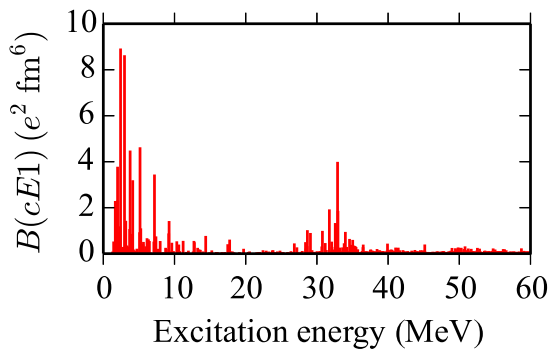

FIG. 11. (Color online) Compressional electric dipole strength of ^{6}He as a function of the excitation energy.

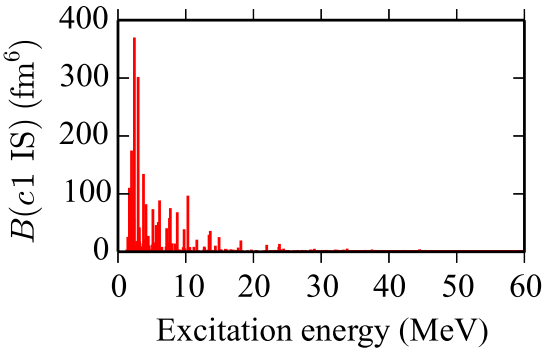

FIG. 12. (Color online) Isoscalar compressional dipole strength of ^{6}He as a function of the excitation energy.

concentrated and enhanced. The SDM is more characterized by the $cE1$ mode rather than the $E1$ one by the additional r^2 factor of the operator. As Eq. (26) suggests, the IS $c1$ mode disappears at the GDR region because of the cancellation of the proton and neutron transition densities. As shown in Fig. 12, the IS $c1$ strength shows up only in the low-energy region and has a strong peak at 2.4 MeV. A measurement of the IS $c1$ mode is of particular interest in relation to the SDM. One possible way to excite the IS $c1$ mode is inelastic α scatterings, ^{6}He$(\alpha,\alpha')^6$He(1^-).

IV. CONCLUSIONS

We have performed a fully microscopic six-body calculation to explore the electric dipole excitation mode in ^{6}He. The ground state wave function is expressed with the explicitly correlated Gaussians. The model space responsible for the $E1$ excitation is also expressed as a combination of the correlated Gaussians with the global vector. The model space explicitly incorporates the configurations for describing the single-particle excitation as well as the final state correlations of $\alpha + n + n$ and $t + d + n$ decay channels.

The ground state properties of the two-neutron separation energy and matter and proton radii and the low-lying $E1$ strength are all reproduced consistently with the observations. The ground state structure is well understood with the $\alpha + n + n$ three-body model though a few-percent core swelling is produced by the halo neutrons.

It is found that the $E1$ non-energy-weighted sum rule is fully accounted for by our model space. The $E1$ strength function exhibits two-peak structure at around 3 and 33 MeV excitation energy. The lower peak is well understood in the framework of the $\alpha + n + n$ structure and its excitation mechanism is consistent with the classical interpretation of the soft dipole mode (SDM), in which in-phase proton-neutron oscillation occurs in the internal region whereas out-of-phase oscillation occurs in the surface region. Beyond the surface region the neutron transition density extends to large distances. The higher peak is the typical giant dipole resonance that exhibits out-of-phase proton-neutron oscillation in the whole region. Just a few MeV above the SDM peak, some new modes are found that can be regarded as a vibrational excitation of the SDM. A measurement for such mode is interesting. We find out that the SDM may be more apparently disclosed by the isoscalar compressional dipole transition rather than the $E1$ transition, and point out the possibility of observing it by inelastic α scatterings.

In this study, we have succeeded to describe, in a single scheme, the $E1$ excitation in a wide energy region from pigmy to giant dipole resonance. It is interesting to extend it to other multipoles or systems to explore other new modes.

ACKNOWLEDGMENT

The work was in part supported by JSPS KAKENHI Grant No. 24540261 and No. 25800121.

[1] I. Tanihata, H. Hamagaki, O. Hashimoto, Y. Shida, N. Yoshikawa, K. Sugimoto, O. Yamakawa, T. Kobayashi, and N. Takahashi, Phys. Rev. Lett. **55**, 2676 (1985).
[2] I. Tanihata *et al.*, Phys. Lett. B **160**, 380 (1985).
[3] I. Tanihata, Phys. Lett. B **206**, 592 (1985).
[4] K. Tanaka *et al.*, Phys. Rev. Lett. **104**, 062701 (2010).
[5] T. Aumann *et al.*, Phys. Rev. C **59**, 1252 (1999).
[6] T. Nakamura *et al.*, Phys. Rev. Lett. **96**, 252502 (2006).
[7] N. Kobayashi *et al.*, Phys. Rev. C **86**, 054604 (2012).
[8] P. G. Hansen and B. Jonson, Europhys. Lett. **4**, 409 (1987).
[9] K. Ikeda, INS Report No. (1988) (in Japanese).
[10] Y. Suzuki, K. Ikeda, and H. Sato, Prog. Theor. Phys. **83**, 180 (1990).
[11] M. Goldhaber and E. Teller, Phys. Rev. **74**, 1046 (1948).
[12] H. Steinwedel, J. H. D. Jensen, and P. Jensen, Phys. Rev. **79**, 1019 (1950).
[13] L. W. Chen, C. M. Ko, B. A. Li, and J. Xu, Phys. Rev. C **82**, 024321 (2010).
[14] T. Inakura, T. Nakatsukasa, and K. Yabana, Phys. Rev. C **88**, 051305(R) (2013).
[15] S. Nakayama *et al.*, Phys. Rev. Lett. **85**, 262 (2000).
[16] Y. Suzuki, Nucl. Phys. A **528**, 395 (1991).
[17] B. V. Danilin, T. Rogde, S. N. Ershov, H. Heiberg-Andersen, J. S. Vaagen, I. J. Thompson, and M. V. Zhukov, Phys. Rev. C **55**, R577 (1997).
[18] T. Myo, K. Kato, S. Aoyama, and K. Ikeda, Phys. Rev. C **63**, 054313 (2001).
[19] D. Baye, P. Capel, P. Descouvemont, and Y. Suzuki, Phys. Rev. C **79**, 024607 (2009).
[20] K. Hagino, H. Sagawa, T. Nakamura, and S. Shimoura, Phys. Rev. C **80**, 031301(R) (2009).
[21] E. C. Pinilla, D. Baye, P. Descouvemont, W. Horiuchi, and Y. Suzuki, Nucl. Phys. A **865**, 43 (2011).
[22] K. Arai, Y. Suzuki, and R. G. Lovas, Phys. Rev. C **59**, 1432 (1999).
[23] S. Bacca, M. A. Marchisio, N. Barnea, W. Leidemann, and G. Orlandini, Phys. Rev. Lett. **89**, 052502 (2002).
[24] S. Bacca, N. Barnea, W. Leidemann, and G. Orlandini, Phys. Rev. C **69**, 057001 (2004).

[25] D. R. Thompson, M. LeMere, and Y. C. Tang, Nucl. Phys. A **286**, 53 (1977).
[26] K. Varga and Y. Suzuki, Phys. Rev. C **52**, 2885 (1995).
[27] I. Reichstein and Y. C. Tang, Nucl. Phys. A **158**, 529 (1970).
[28] K. Varga, Y. Suzuki, and Y. Ohbayasi, Phys. Rev. C **50**, 189 (1994).
[29] W. Horiuchi and Y. Suzuki, Few-Body Syst. **54**, 2407 (2013).
[30] S. F. Boys, Proc. R. Soc. London Ser. A **258**, 402 (1960).
[31] K. Singer, Proc. R. Soc. London Ser. A **258**, 412 (1960).
[32] W. Horiuchi and Y. Suzuki, Phys. Rev. C **78**, 034305 (2008).
[33] W. Horiuchi and Y. Suzuki, Phys. Rev. C **89**, 011304(R) (2014).
[34] J. Mitroy, S. Bubin, W. Horiuchi, Y. Suzuki, L. Adamowicz, W. Cencek, K. Szalewicz, J. Komasa, D. Blume, and K. Varga, Rev. Mod. Phys. **85**, 693 (2013).
[35] Y. Suzuki and K. Varga, *Stochastic Variational Approach to Quantum-Mechanical Few-Body Problems*, Lecture Notes in Physics Vol. m54 (Springer, Berlin, 1998).
[36] K. Varga, Y. Suzuki, and R. G. Lovas, Nucl. Phys. A **571**, 447 (1994).
[37] Y. Suzuki, W. Horiuchi, M. Orabi, and K. Arai, Few-Body Syst. **42**, 33 (2008).
[38] S. Aoyama, K. Arai, Y. Suzuki, P. Descouvemont, and D. Baye, Few-Body Syst. **52**, 97 (2012).
[39] W. Horiuchi, Y. Suzuki, and K. Arai, Phys. Rev. C **85**, 054002 (2012).
[40] W. Horiuchi and Y. Suzuki, Phys. Rev. C **87**, 034001 (2013).
[41] G. Audi, A. H. Wapstra, and C. Thibault, Nucl. Phys. A **729**, 337 (2003).
[42] R. Goerke, S. Bacca, and N. Barnea, Phys. Rev. C **86**, 064316 (2012).
[43] I. Angeli and K. P. Marinova, At. Data Nucl. Data Tables **99**, 69 (2013).
[44] M. Brodeur *et al.*, Phys. Rev. Lett. **108**, 052504 (2012).
[45] L.-B. Wang *et al.*, Phys. Rev. Lett. **93**, 142501 (2004).
[46] G. D. Alkhazov *et al.*, Phys. Rev. Lett. **78**, 2313 (1997).
[47] I. Tanihata, D. Hirata, T. Kobayashi, S. Shimoura, K. Sugimoto, and H. Toki, Phys. Lett. B **289**, 261 (1992).
[48] O. A. Kiselev *et al.*, Eur. Phys. J. A **25**, 215 (2005)
[49] S. Bacca, N. Barnea, and A. Schwenk, Phys. Rev. C **86**, 034321 (2012).
[50] W. Horiuchi and Y. Suzuki, Phys. Rev. C **76**, 024311 (2007).
[51] D. R. Tilley, C. M. Cheves, J. L. Godwin, G. M. Hale, H. M. Hofmann, J. H. Kelley, C. G. Sheu, and H. R. Weller, Nucl. Phys. A **708**, 3 (2002).
[52] A. Csótó, Phys. Rev. C **49**, 3035 (1994).
[53] Y. Alhassid, M. Gai, and G. F. Bertsch, Phys. Rev. Lett. **49**, 1482 (1982).
[54] H. Sagawa and M. Honma, Phys. Lett. B **251**, 17 (1990).
[55] Y. Suzuki and Y. Tosaka, Nucl. Phys. A **517**, 599 (1990).
[56] D. R. Tilley, H. R. Weller, and G. M. Hale, Nucl. Phys. A **541**, 1 (1992).
[57] I. J. Thompson and M. V. Zhukov, Phys. Rev. C **49**, 1904 (1994).
[58] K. Varga, Y. Suzuki, and R. G. Lovas, Phys. Rev. C **66**, 041302(R) (2002).
[59] T. Myo, K. Kato, H. Toki, and K. Ikeda, Phys. Rev. C **76**, 024305 (2007).
[60] Y. Kikuchi, T. Myo, K. Kato, and K. Ikeda, Phys. Rev. C **87**, 034606 (2013).
[61] T. Inakura, W. Horiuchi, Y. Suzuki, and T. Nakatsukasa, arXiv:1405.7888 [Phys. Rev. C (to be published)].
[62] S. Stringari, Phys. Lett. B **108**, 232 (1982).